Authors

Daniel W McKay[1], Yue Qu[1], Heather E McFarlane[2,3], Apriadi Situmorang[1], Matthew Gilliham[1] and Stefanie Wege[1,*]

Affiliations

[1]ARC Centre of Excellence in Plant Energy Biology, PRC, School of Agriculture, Food and Wine, Waite Research Institute, University of Adelaide, Waite Campus, Glen Osmond 5064, South Australia, Australia

[2]School of Biosciences, University of Melbourne, Melbourne, VIC 3010, Australia

[3]Present address: Department of Cell and Systems Biology, University of Toronto, Toronto, ON, M5S 3G5, Canada

[*]Correspondence: stefanie.wege@adelaide.edu.au

Title

Cation Chloride Cotransporter 1 (CCC1) regulates pH and ionic conditions in the TGN/EE and is required for endomembrane trafficking

Running title

TGN/EE ion and pH regulation by CCC1

One sentence summary

The TGN/EE-localised Cation Chloride Cotransporter 1 maintains optimal luminal ionic and pH conditions required for intracellular protein trafficking and cell elongation.

Abstract

The secretory and endocytic pathways intersect at the Trans-Golgi Network/Early Endosome (TGN/EE). TGN/EE function depends on luminal pH adjustment, which is regulated by the combined activity of a proton pump and several proton/ion antiporters. The identity of the proton pump is known, as well the antiporters that catalyse cation and anion import into the TGN/EE. However, the protein(s) required to complete the transport circuit, and that mediates cation and anion efflux has not been identified. Here, we characterise Arabidopsis Cation Chloride Cotransporter (AtCCC1) and show that it is localised in the TGN/EE. We further demonstrate that regulation of both luminal pH and ion concentrations are dependent on AtCCC1 function, using pharmacological treatments and genetically encoded fluorescent sensors. Loss of AtCCC1 leads to alterations in cellular functions dependent on the TGN/EE including endo- and exocytosis, trafficking to the vacuole and trafficking of the plasma membrane protein PIN2. This discovery provides the cellular role for CCC1s and can explain the multitude of phenotypic defects observed in loss-of-function plants. Collectively, our results demonstrate that non-proton-coupled ion transport contributes to the regulation of TGN/EE luminal ionic and pH conditions; and that CCC1 is an essential missing component of the TGN/EE ion transport circuit.

Introduction

In plants, the secretory and endocytic pathways intersect at a single organelle, the *Trans*-Golgi Network/Early Endosome (TGN/EE). The TGN/EE, therefore, plays a vital role in sorting of newly synthesised proteins and endocytosed cargo (Dettmer et al., 2006; Viotti et al., 2010; Sze and Chanroj, 2018). The complex cellular function of the TGN/EE is thought to depend on a finely tuned luminal pH, and potentially luminal ion composition (Martinière et al., 2013; Luo et al., 2015; Reguera et al., 2015). Within the endomembrane system, the TGN/EE has been shown to contain the most acidic luminal pH, which is established by the TGN/EE localised V-H^+-ATPase (Martinière et al., 2013). Plants with reduced TGN/EE V-H^+-ATPase activity, called *det3*, exhibit strong developmental growth defects, suggesting that the low luminal pH is crucial for plant growth and development (Schumacher et al., 1999). The contribution of V-H^+-ATPase to the acidification of the TGN/EE was confirmed with genetically encoded pH sensors, and these alterations of TGN/EE luminal pH in *det3* plants

impacts the function of this organelle as demonstrated by the missorting of the plasma membrane (PM) protein BRI1 (Luo et al., 2015).

In addition to the V-H^+-ATPase, pH regulation is also dependent on the activity of cation/proton exchangers (= antiporters). Proton-coupled cation transport is thought to be crucial for the fine-tuning of luminal pH. The activity of cation proton exchangers provides an electroneutral proton efflux pathway, in addition to cation import into the TGN/EE lumen. The best characterised ion transporters in the TGN/EE are the cation/proton exchangers NHX5 and NHX6. Double *nhx5 nhx6* mutants have similar, but not identical, growth defects to *det3* (Bassil et al., 2011; Reguera et al., 2015). Both mutants display reduced cell length, and a large decrease to overall plant size. However, in contrast to what was found in *det3*, the *nhx5/nhx6* TGN/EE lumen is hyperacidic, which is consistent with the proposed role of NHX in exporting protons (Luo et al., 2015; Reguera et al., 2015). Like in *det3*, trafficking of BRI1 is also altered in *nhx5/nhx6*; however only recycling is affected while sorting to the PM is not (Dragwidge et al., 2019). Similarly, sorting of other membrane integrated proteins such as PIN2 is also unaffected in *nhx5/nhx6* (Dragwidge et al., 2018). Additionally, the hyperacidity of *nhx5/nhx6* TGN/EE lumen results in missorting of vacuolar proteins due to altered binding of targets by the Vacuolar Sorting Receptor VSR1;1 (Reguera et al., 2015). These results indicate that alkalinisation and hyperacidification of the TGN/EE lumen lead to similar but distinct defects, highlighting the importance of a tight regulation of luminal conditions in the TGN/EE for normal plant growth and development.

In animals, chloride/proton antiporters of the CLC protein family are important for lysosome acidification. This function is reliant on the coupled transport of protons and anions. A variant of CLC with anion transport un-coupled from proton transport was unable to complement the *clc-5* knockout mice phenotype of increased lysosomal pH, highlighting the importance of this proton coupled transport (Novarino et al., 2010). In plants, two members of the CLC family are localised in the Golgi and TGN/EE, CLCd and CLCf (Marmagne et al., 2007; von der Fecht-Bartenbach et al., 2007). CLCd is important for pathogen resistance, with otherwise little developmental growth defects in the single *clcd* knockout (Guo et al., 2014). It has been suggested that CLCd and CLCf fulfil similar roles to their animal homologues, but this remains to be tested (Sze and Chanroj, 2018). They might also fulfil partially redundant roles, as is the case of NHX5 and NHX6; but no *clcd clcf* double knockout has been described so far so this cannot be concluded yet.

Collectively, the above outlined transport processes account for the current model of regulation of pH and ions in the TGN/EE lumen. This current model is incomplete as it does not yet contain a transport protein that mediates either cation or anion efflux. Here, we have explored a lead provided by previous findings that suggest CCC1 is localised to the endomembrane system; with heterologous expression studies and proteomics in Arabidopsis identifying it as localised to the TGN/EE. CCC1s mediate electroneutral cation and anion symport, and are therefore excellent candidates to provide an ion efflux mechanism (Colmenero-Flores et al., 2007; Nikolovski et al., 2012; Henderson et al., 2015). Arabidopsis contains a single *CCC gene*, *AtCCC1*. *Atccc1* knockouts exhibit a complex and severe phenotype, suggesting that AtCCC1 is required for a core cellular function (Colmenero-Flores et al., 2007; Han et al., 2020). *Atccc1* plants show large reductions in overall plant size, have a bushy appearance characterised by an increased axillary shoot outgrowth, frequent stem necrosis, very low fertility, alterations in pathogen response, and changes in cell wall composition (Johnson et al., 2004; Colmenero-Flores et al., 2007; Henderson et al., 2018; Han et al., 2020) .

Here, we demonstrate that the non-proton coupled ion transporter, AtCCC1, is required for the regulation of the TGN/EE luminal pH for the efflux of ions, and that loss of function leads to defects in TGN/EE dependent processes. This includes alterations in trafficking of the auxin transporter PIN2 and the PM marker LTI6b, and trafficking of endocytosed cargo to the vacuole. We propose that AtCCC1 impacts these processes because it is the missing component of the ion and pH regulating machinery of the TGN/EE.

Results

AtCCC1 *is ubiquitously expressed.*

Reports on *AtCCC1* expression are somewhat contradictory. Promoter-GUS studies indicated that *AtCCC1* expression is restricted to specific tissues, such as root stele or hydathodes and pollen; while RNA transcriptomic studies, including single-cell RNAseq, suggest expression occurs in other cell types as well (Colmenero-Flores et al., 2007; Wendrich et al., 2020). To clarify the tissue expression pattern of *AtCCC1*, we transformed Col-0 wildtype plants with a 2kb genomic DNA sequence upstream of the *AtCCC1* coding region driving the expression

of nuclear localised triple Venus (a bright variant of the yellow fluorescent protein) or β-glucuronidase (GUS, named *AtCCC1prom::Venus* and *AtCCC1prom::GUS*, respectively). Combined analysis of fluorescence and GUS-staining revealed that *AtCCC1* is expressed in all cell types, including all root cells, hypocotyl, leaf and stem epidermis, guard cells and trichomes, as well as mesophyll cells and all flower parts, with a particularly strong signal in stamen filaments (Fig. 1). *AtCCC1* promoter activity reported by Venus fluorescence, or by GUS-activity, was slightly different despite use of the identical promoter sequence. For instance, fluorescence was detectable in root cortex and epidermis cells, including root hairs, and in the gynoecium, while GUS staining did not indicate expression in these cells. This is likely due to the increased sensitivity of the Venus fluorescence method.

CCC1 is important for cell elongation

Our expression analysis showed that *AtCCC1* is expressed in all root cells (Fig. 1), and AtCCC1 was previously shown to be important for primary root growth (Colmenero-Flores et al., 2007; Henderson et al., 2015). We investigated the root knockout phenotype for alteration on the cellular level, of plants grown in vitro on ½ MS. We found that AtCCC1 function is required for cell elongation, and knockouts develop shorter root epidermis cells. *Atccc1* additionally develops shorter root hairs and has a complete lack of collet hairs, which are epidermal root hairs formed in some plant species in the transition zone between the root and the hypocotyl (Fig. 2) (Sliwinska et al., 2015). To investigate the cause of the reduced root hair length in *Atccc1*, the elongation rates of wildtype and *Atccc1* root hairs were measured using time lapse microscopy (suppl. Videos 1-2). For this, roots were grown inside the media, in chambered cover slips. The elongation rate of wildtype plants in our conditions was similar to what had previously been observed (Schoenaers et al., 2018). Measurements revealed that *Atccc1* root hairs were shorter because they grow at a reduced speed, no premature growth arrest was detected. Between 50 and 100 minutes after elongation initiated, wildtype root hairs had an average elongation rate of 0.88 ± 0.27 µm min^{1-}, while *Atccc1* root hairs elongated at half that speed, with0.47 ± 0.08 µm min^{1-} (Fig. 2). In addition, *Atccc1* root hairs also displayed branching and bulging, although, at a low frequency (Fig. S1). Ruptured root hairs were never observed (suppl. Fig. S1). Independent of the defect of root hair cell elongation, *Atccc1* plants frequently developed root hairs in cell files that usually exclusively contain atrichoblasts. Root hair cell identify was confirmed using the trichoblast marker

PRP3::H2B-2xmCherry (Marques-Bueno et al., 2016); this showed the frequent presence of multiple adjacent trichoblasts (Fig. S1)(Marques-Bueno et al., 2016).

AtCCC1 *localises to the endomembrane system in root hair cells*

We had previously localised AtCCC1-GFP to the Golgi and TGN/EE in transient expression assays in *N. benthamiana* (Henderson et al., 2015). In contrast, other studies have suggested that AtCCC1 might localise to the PM. This has led to multiple interpretations of AtCCC1 function (Henderson et al., 2015; Wegner, 2017; Domingos et al., 2019). To clarify the subcellular localisation of AtCCC1, we generated plants that stably express N-terminally tagged GFP-AtCCC1 using the *EXP7* (*Expansin7*) root hair specific promoter. This approach was adopted after many attempts to generate plants with native *AtCCC1* promoter driven expression, which did not produce any transformants. The approaches taken included use of different linkers, fluorescent proteins, smaller tags such as FLAG-tag, and both N- and C-terminal tagging. The difficulty in obtaining transformed plants might suggest that tagging interferes with AtCCC1 function in embryonic or meristematic tissue where it is highly expressed (Fig. 1). We therefore decided to express GFP-AtCCC1 in a mature cell type, in which we had identified a clear phenotypic defect in *Atccc1*, root hair cells. Root hair specific expression was successful and importantly, complemented the short root hair phenotype of *Atccc1* knockout plants (Fig 3).

Stable expression of GFP-AtCCC1 in a native cell type revealed a similar pattern to what we observed in *N. benthamiana* and the GFP signal was localised to internal organelles resembling components of the endomembrane system (Henderson et al., 2015). Time lapse imaging of the movement of GFP-AtCCC1 signal in root hairs and trichoblasts was consistent with what could be expected for the Golgi or TGN/EE, however, GFP-AtCCC1 labelled organelles did not resemble the Golgi (suppl. Videos V2 and V3). To identify the observed GFP-AtCCC1 labelled compartments, we crossed the stably expressed marker VHAa1-RFP into plants expressing GFP-AtCCC1 (Dettmer et al., 2006). Stable co-expression revealed that the majority of AtCCC1 colocalises with the TGN/EE marker (Fig. 3). Colocalisation of GFP-AtCCC1 and VHAa1-RFP was measured by calculating the Pearson correlation coefficient of pixel signal intensity for RFP and GFP channels, which gave a value of 0.86±0.055 (Bolte and Cordelieres, 2006). Object based colocalisation analysis, using the ImageJ plugin DiAna, revealed that 73±9% of VHAa1-RFP colocalise

with GFP-AtCCC1, indicating a very high degree of colocalisation, while 58±11% of GFP-AtCCC1 colocalised with VHAa1-RFP (Gilles et al., 2017), The asymmetrical colocalisation indicates that, in addition to the TGN/EE, AtCCC1 might also localise to additional organelles of the endomembrane system (Fig. 3). Pharmacological treatment further confirmed the endosomal localisation. Treatment with the trafficking inhibitor, brefeldin-A (BFA), caused the GFP signal to accumulate in the centre of BFA bodies, consistent with a TGN/EE localisation and not Golgi (suppl. Fig. S2). We then investigated, if AtCCC1 shuttles to the PM and back. Other ion transporters have been shown to localise mainly in endosomes, but function at the PM, such as the iron transporter IRT1 (Barberon et al., 2011). PM localisation of IRT1 could be visualised by inhibition of endocytosis, with the endocytosis inhibitor TyrA23. Subcellular localisation of GFP-AtCCC1 remained unchanged after treatment with TyrA23, no signal could be observed at the PM; similarly, an osmotic shock treatment did not lead to any observable changes in GFP-AtCCC1 localisation (suppl. Fig. S2). Combined, our results show very strong evidence that AtCCC1 functions in the TGN/EE.

Loss of other TGN/EE localised proteins, such as the H^{+}-V-ATPase, can affect the TGN/EE morphology (Dettmer et al., 2006). We therefore investigated organelle ultrastructure in *Atccc1*. High-pressure freezing, freeze substitution, and transmission electron microscopy revealed that the lack of AtCCC1 does not lead to obvious morphological changes in the TGN/EE ultrastructure, and the appearances of all organelles was similar between *Atccc1* mutants and wildtype (suppl. Fig. S3). The defects observed in *Atccc1* knockouts might therefore be connected to changes in TGN/EE luminal conditions.

AtCCC1 is required for regulation of luminal ion composition and pH in the TGN/EE

To investigate a possible role of AtCCC1 in adjusting TGN/EE lumen conditions, we utilised pharmacological treatment to investigate ion transport, and introduced stably expressed TGN/EE localised genetically encoded fluorescent pH sensors (SYP61-pHusion) in *Atccc1* (Luo et al., 2015).

To assess if the loss of AtCCC1 results in changes to the ability of the TGN/EE to maintain a stable luminal environment, the ionophore monensin was utilised. Monensin is a monovalent cation ionophore, acting as a membrane permeable ion exchanger, exchanging luminal protons for cations (Zhang et al., 1993). This rapid increase in osmotically active cations

leads to observable TGN/EE swelling. The action of monensin is therefore partly dependent on the pH gradient between the TGN/EE and the cytosol. In addition, the cation concentration gradient might also plays a role, because *nhx5 nhx6* mutants are less sensitive to monensin induced TGN/EE swelling despite a more acidic luminal pH (Dragwidge et al., 2019). We hypothesised that AtCCC1 is important for ion efflux out of the TGN/EE and therefore *Atccc1* TGN/EE might be hypersensitive to monensin induced TGN/EE swelling. We assessed the susceptibility of *Atccc1* to monensin using live-cell imaging of VHAa1-RFP labelled TGN/EE in wildtype and *Atccc1* cells in the root elongation zone, treated with 2.5 µM of monensin for 15 minutes. In 15 minutes, the average wildtype TGN/EE size increased by 28% ±13% while *Atccc1* TGN/EE size increased by 52% ±16%, revealing a highly increased susceptibility of *Atccc1* TGN/EE lumen to osmotically induced swelling due to cation accumulation (Fig. 4). This suggests that AtCCC1 mitigates the effect of monensin in wildtype by effluxing K^+ and Cl^-, as anion and cation transport are stochiometrically linked in AtCCC1.

To investigate if defects in cation-anion symport can impact the pH regulation in the TGN/EE, we introduced the stably expressed TGN/EE localised pH-sensor pHusion into *Atccc1* (Luo et al., 2015). Confocal imaging of epidermal cells in the root elongation zone revealed that luminal pH is more alkaline in *Atccc1,* with a pH of 5.8 ±0.05, compared to wildtype with a pH of 5.5 ±0.05 (Fig. 4). In addition, we measured vacuolar pH in wildtype and *Atccc1* using the pH sensitive dye, BCECF. No difference was found between the genotypes, suggesting that lack of AtCCC1 does not impact vacuolar pH but leads to spatially defined pH changes (Fig. S3).

Loss of AtCCC1 results in defects of endomembrane trafficking

Since pH and ion homeostasis are essential to TGN/EE function, we next investigated whether rates of endomembrane trafficking was altered in plants with a lack of AtCCC1. We selected epidermal cells in the root elongation zone for imaging, similar to those used for imaging for pH and monensin measurements.

The rate of protein recycling and exocytosis was assayed using wildtype and *Atccc1* stably expressing PIN2-GFP or the PM-marker GFP-LTI6b (Cutler et al., 2000; Xu and Scheres, 2005). Roots were treated first with BFA before a subsequent washout (Cutler et al., 2000; Xu and Scheres, 2005). BFA treatment resulted in the accumulation of these fluorescently tagged proteins in the endomembrane system due to a block in exocytosis and recycling to

the PM. This is measured as a strong increase in the cytoplasmic GFP signal relative to the PM signal (cytoplasmic:PM ratio). This increased ratio was observed for both proteins, demonstrating that BFA-induced inhibition of exocytosis worked on both the wildtype and mutant, and that proteins were retained in the endomembrane system (Fig. 5). In addition to an inhibition of exocytosis, BFA treatment in Arabidopsis root cells can also lead to the formation of BFA bodies, which are an amalgamation of Golgi and TGN/EE (Geldner et al., 2001). We typically observed fewer BFA bodies in *Atccc1* compared to the wildtype, however, this did not affect the accumulation of intracellular GFP signal in the knockout. Upon BFA washout, recycling and secretion to the plasma membrane is resumed, enabling the rate of exocytosis to be measured. Exocytosis is measured as the rate that the endomembrane accumulated GFP-signal decreases and PM signal increases, which results in a decreased cytoplasmic:PM signal ratio.

Prior to BFA treatment, we measured similar cytoplasmic:PM ratios for PIN2-GFP in both wildtype and *Atccc1* plants (Fig. 5, T0). The 60 minutes of 25 µM BFA treatment caused a slightly higher increase in the cytoplasmic:PM ratio in wildtype and *Atccc1*. 60 minutes after washout of the BFA, the wildtype plants exhibited an almost complete recovery of the cytoplasmic:PM ratio back to the state before BFA treatment. In contrast, *Atccc1* showed minimal recovery in the cytoplasmic:PM ratio indicating a considerable decrease in the rate at which PIN2-GFP is exocytosed to the PM (Fig. 5). Similar experiments using GFP-LTI6b revealed that in the wildtype background, the initial ratio of cytoplasmic:PM fluorescence was very low, indicating that most of the proteins were at the PM, consistent with the use of LTI6b as a PM-marker (Fig. S4). This was in contrast to *Atccc1*, where the cytoplasmic:PM fluorescence ratio was already very high before treatment, indicating an increased percentage of LTI6b inside the cell (Fig. S4). After 60 minutes of treatment with BFA, the GFP signal was internalised in all genotypes, however, as the cell-internal signal in *Atccc1* was already high before treatment, the impact of BFA was minimal (Fig. S4). The substantial percentage of PM-marker LTI6b inside the cells in *Atccc1* without treatment suggest a general defect with exocytosis in *Atccc1*.

Defects in exocytosis and protein cycling are often accompanied by changes in endocytosis, which we therefore also measured in *Atccc1*. Endocytosis was measured by the internalisation of the endocytic tracer FM4-64, both with and without the exocytosis inhibitor BFA. FM4-64 internalisation was measured by an increase in the cytoplasmic:PM signal ratio, similar to the exocytosis assay. After 10 minutes of combined treatment with FM4-

64/BFA, *Atccc1* cells showed a lower fluorescent ratio when compared to wildtype (Fig. 5). After 60 minutes of treatment (10 minutes with FM4-64/BFA, 50 minutes with BFA only), this difference increased further and the fluorescent ratio was much lower in *Atccc1* than wildtype, indicating a large reduction in the rate of endocytosis.

In a second time course experiment, trafficking of FM4-64 to the vacuole was measured, without the use of BFA. Labelling of the tonoplast with FM4-64 became visible in both wildtype and mutant after 3 hours. The ratio of tonoplast:PM fluorescence revealed that *Atccc1* had a reduced ratio of tonoplast:PM FM4-64 signal when compared to wildtype, indicating a reduction in the trafficking of endocytosed FM4-64 to the vacuole (Fig. 5).

Discussion

Here, we show that *AtCCC1* is ubiquitously expressed and demonstrate that the AtCCC1 protein is localised to the endomembrane system and not the PM, with the majority of the protein localising in the TGN/EE. The expression pattern of *AtCCC1* is similar to rice (*Oryza sativa*) *OsCCC1.1* expression. Also similar to observation from *Osccc1.1* loss-of-function plants, AtCCC1 function is required for cell elongation, and knockouts develop shorter root epidermis cells and root hairs, as well as root hairs in cell files adjacent to each other (Fig. 2, Fig. S1) (Chen et al., 2016). The short root hair phenotype of *Atccc1* is complemented by *EXP7*-promoter driven expression of GFP-AtCCC1, while the alterations in trichoblast patterning is not. This is consistent with the use of the *EXP7*-promoter, with an onset expression after cell identity is already conferred, and suggests that the cause of altered cell identify is due to loss of AtCCC1 function in cell of the root tip. The similarity of the overall loss-of-function phenotypes observed between *Atccc1* and *Osccc1.1*, and the ability of the grapevine homologue *VvCCC1* to complement *Atccc1*, indicates that CCC1 function may be conserved across plant species (Henderson et al., 2015). However, until now, there was no mechanistic explanation for the observed phenotypes.

We show that AtCCC1 is localised in the TGN/EE in Arabidopsis, and loss of AtCCC1 function leads to defects in establishing the typical, low pH in TGN/EE lumen, and to defects in counteracting the cation induced osmotic swelling of TGN/EE by monensin (Fig. 4). This suggests that AtCCC1 is important for regulation of pH and ions. In the TGN/EE, both hyperacidification and a more alkaline pH lead to changes in membrane trafficking cell expansion and cell wall formation and possibly pathogen response, indicating that the pH is

strictly regulated. The pH regulation in the TGN/EE is dependent on activity of the V-H+-ATPase, NHX5, NHX6, and likely CLCd (Dettmer et al., 2006; Brux et al., 2008; Guo et al., 2014; Reguera et al., 2015).. In addition, the potassium efflux antiporters KEA4, KEA5 and KEA6 are also localised in the TGN/EE and might contribute to luminal pH regulation, yet their role is currently less understood and triple knockouts show a much less severe phenotype compared to *nhx5 nhx6* (Wang et al., 2019). In agreementwith a role in pH regulation, we found that AtCCC1 is important for membrane trafficking, exocytosis and protein recycling of the proteins PIN2 and LTI6b, and for PM-vacuole trafficking.

Our combined results give evidence that CCC1s are the missing component in the pH transport circuit in the TGN/EE, and are the first proteins identified to provide a cation and anion efflux pathway (Fig. 6). Interestingly, AtCCC1 is an anion cation symporter, which fixes the stoichiometry of exported anion and cations to 1:1. This ion export ratio might tightly connect the activities of the ion exchangers, and contribute to the strict regulation of pH.

Functional endomembrane transport has a vital role in many cellular processes, including cell wall formation, nutrient acquisition and the establishment of hormone gradients; and AtCCC1 might play a role in all of them. Cell wall polysaccharides are synthesised in the endomembrane system and then depend on regulated transport to the PM (Sinclair et al., 2018). Interestingly, *Atccc1* plants were recently found to exhibit alterations in cell wall composition, confirming the connection of endomembrane ion transporters and cell wall formation (Han et al., 2020). Auxin transporters, and the downstream auxin maxima, are frequently shown to be affected in plants with impaired endomembrane transport (Adamowski and Friml, 2015); and we found alterations of PIN2 cycling in *Atccc1* (Fig. 5). *Atccc1* plants have a strikingly bushy appearance, which might be connected to alteration in auxin distribution.

Nutrient uptake and translocation is also affected in plants with defects in endomembrane ion transport (Guan et al., 2014); possibly through indirect alterations of ion transporters in the PM and tonoplast, which depend on a regulated trafficking and sorting to their respective destination. In addition, some transporters such as IRT1 regularly cycle between the PM and internal compartments, which will likely be affected in plants with defects in endomembrane trafficking (Barberon et al., 2011). In agreement with this, *Atccc1* shows changes in total shoot K^+, Na^+ and Cl^- accumulation (Colmenero-Flores et al., 2007; Henderson et al., 2015);

and AtCCC1 was identified in a screen investigating the seed ionome, with *Atccc1* seeds showing a strong increase in Fe, Ca^{2+} and SO_4^{2-}, and a decrease in K^+ and Na^+ (McDowell et al., 2013). The alterations in Fe, Ca^{2+} and SO_4^{2-} are of interest as these are not substrates of AtCCC1. Further research is required to investigate the role of ion transporters in the endomembrane system, their connection to nutrient transporter localisation, and ion fluxes across other membranes.

Material and Methods

Plant material and growth conditions

Arabidopsis thaliana were all in the Columbia-0 (Col-0) background. Previously described T-DNA insertion lines in AT1G30450, *Atccc1-1* (SALK-048175) and *Atccc1-2* (SALK-145300) were used in this study (Colmenero-Flores et al., 2007). *PIN2::PIN2-GFP, 35S::VHAa1-RFP, 35S::GFP-LTIB6 and 35s::SYP61-pHusion* plant lines were previously described (Cutler et al., 2000; Xu and Scheres, 2005; Dettmer et al., 2006; Luo et al., 2015).

Arabidopsis plants were grown on media containing half strength Murashige and Skoog (1/2 MS) 0.1% sucrose, 0.6% phytagel, pH 5.6 with KOH. Plants were sown on plates, incubated at 4°C for at least 2 days and subsequently grown vertically at 21°C and 19°C in 16 h light and 8 h dark, respectively. Plants were grown for different periods of time, as indicated below and stated in the figure legends.

Promoter activity analysis by GUS and Venus fluorescence

GUS staining was done according to Jefferson et al. (1987). In summary, plants with the ages indicated in figure legend 1 were submerged in GUS-staining solution and stained for the times indicated in figure legend 1. Image of the entire rosette was captured with a Nikon digital camera, flower and inflorescence images with a Nikon SMZ25 stereo microscope. Fluorescence of the nuclear localised NLS-Venus was imaged in plants ranging from 5-8 d to 8 weeks as indicated in figure legend 1. Excitation light wavelength was 514 nm, emission was detected at 520-560 nm, using either a Nikon A1R or a Olympus FV3000 Confocal Laser-Scanning Microscope; with the following objectives: 20x Plan Apo Lambda and 40x Apo LWD WI Lambda S (Nikon), and 10x UPSLAPO objective (Olympus).

Root hair length, root hair elongation rate

Light microscopy imaging of root hair length was performed using a Nikon SMZ25 stereo microscope with a 2x objective. For quantification of root hair length, images of roots were taken from above the maturation zone of 6 day old plants. Each measurement was of a single root hair. Multiple root hairs were measured per plant. Root hair length was measured using FIJI (Schindelin et al., 2012). For time lapse light microscopy of root hair elongation rate, plants were germinated within 2 mL of media placed in 1-well microscopy slides (Thermo Fisher) and grown vertically. Images of root hairs in the maturation zone were taken every 30 seconds for 6 hours using a Nikon Diaphot 300. Measurements were taken from the beginning of root hair elongation, of root hairs that elongated beyond the initiation phase, until root hair growth ceased. For consistency, elongation rates of root hairs were only measured for root hairs where both initiation and cessation of growth could be observed in the time lapse. A single root hair was measured per plant. Analysis and creation of videos was performed using FIJI.

Root morphology imaging

Root morphology images for epidermal cell length and ectopic root hairs were taken at the same Nikon confocal, using 6 days old seedlings and root cell wall autoflorescence (excitation = 404 nm, emission = 425 - 475 nm). Each measurement for epidermal cell length was of a single cell. Multiple cells were measured per plant.

GFP-AtCCC1 cloning and expression

For stable expression of AtCCC1 in root hairs, 1402 bp of the trichoblast specific promoter *EXP7* (Marquès Bueno et al., 2016) was first amplified from Col-0 genomic DNA, using the primers EXP7pro-HindIII_F (*tatacAAGCTTATTACAAAGGGGAAATTTAGGT*) and EXP7pro-KpnI_R (*cttatGGTACCTCTAGCCTCTTTTTCTTTATTC*), following a Phusion® PCR protocol (NEB). PCR product and the binary plasmid pMDC43 were subsequently cut with the restriction enzymes HindIII-HF and KpnI-HF to remove the *2x35S* promoter, and the digestion reactions were purified using illustra™ GFX™ PCR DNA and Gel Band

Purification kits. Fragment ligation was performed using T4 DNA Ligase protocol (NEB) at $16^{o}C$ overnight. 2 µl of the ligation reaction was transformed into DB3.1 cells and after a sequencing verification, a plasmid was subsequently selected that showed the correct replacement of the *2x35* promoter with the *EXP7* promoter. *AtCCC1* CDS (with stop codon) was then shuttled into the pMDC43EXP7 using LR clonase II enzyme, which creates N-terminally GFP-tagged AtCCC1. Correct plasmids were transformed into *Agrobacterium tumefaciens*, and heterozygous Arabidopsis plants (*Atccc1*$^{+/-}$) were floral dipped as the homozygous *Atccc1* knockout does not support floral dipping well. Floral dipping was performed according to Clough and Bent (1998), and transformants were selected on 1/2 MS plates with no sucrose, containing hygromycin for selection. Homozygous *Atccc1* knockouts expressing the GFP-AtCCC1 were selected, and phenotyped in the next generation.

Colocalisation

For colocalisation, 6 day old plants expressing both GFP-AtCCC1 (excitation = 488 nm, emission = 500 – 550 nm) and the TGN/EE marker VHAa1-RFP (excitation = 561 nm, emission = 570-620 nm) were imaged using Nikon A1R Confocal Laser-Scanning microscope, using a 60x Plan Apo VC WI objective with a numerical aperture of 1.2; pinhole set to of 1.2 AU. Five roots were imaged, with three images of three separate mature epidermal root cells being imaged per plant. Analysis was performed on image stacks with a stepsize of 0.45 µm. Colocalisation was assessed using the FIJI plugin DiAna (Gilles et al., 2017). In brief, segmentation was performed using the iterative segmentation function before the number of objects which overlap are counted. The percentage of overlapping objects is reported as the percentage of colocalisation. Colocalisation with DiAna was supported by obtaining the Pearson's coefficient on the same stacks using JACoP (Bolte and Cordelieres, 2006).

TGN/EE swelling with monensin

TGN/EE swelling was induced using the ionophore, monensin (Sigma). 6 day old plant roots expressing VHAa1-RFP (excitation = 561 nm, emission = 570-620 nm) were submerged in ½ MS solution with or without 2.5 µM monensin for 15 minutes before imaging. Imaging was performed on the Nikon A1R Confocal Laser-Scanning microscope and 60x objective

described above. Images were a single optical section, taken of epidermal cells in the root elongation zone. A single measurement was taken per plant, which included multiple cells. Measuring was done using FIJI. TGN/EE were identified using VHAa1-RFP signal and segmented using the automatic threshold algorithm, “RenyiEntropy”. The average size of the segmented TGN/EE was measured using “Analyse Particles”.

TGN/EE pH measurements

The pH of the TGN/EE was measured as described in Luo et al. (2015). In brief, SYP61-pHusion (excitation 488 and 561 nm, emission 500 – 550 and 570 – 620 nm) was imaged in epidermal cells of the root elongation zone of 6 day old plants on the Nikon A1R Confocal Laser-Scanning microscope and 60x objective described above, obtaining a single optical slice. GFP/RFP intensity ratios are obtained from cells incubated in solutions of known pH to create a calibration curve. TGN/EE pH may then be measured by obtaining ratios from untreated plants. The calibration curve was created by measuring cells treated for 15 minutes with 50 mM MES-BTP (bis-tris-propane) or 50 mM HEPES-BTP with 50 mM ammonium acetate. Seven points between pH 5.0 and 8.0 were measured for the calibration curve. Six measurements were taken per point for calibration and a calibration was performed before every experiment. The curve was fit using a Boltzmann sigmoidal in GraphPad Prism 8.0. A single measurement was taken per plant which included multiple cells. The GFP/RFP ratio was obtained in FIJI by firstly segmenting for TGN/EE using the automatic “RenyiEntropy” threshold on the RFP signal before measuring fluorescent intensity.

Endo- and Exocytosis

Endocytosis was assayed in the root tips of 6 day old plants using the fluorescent membrane stain FM4-64 (excitation = 561 nm, emission = 570 – 620 nm) and the endomembrane trafficking inhibitor brefeldin A (BFA). Plants were either incubated in 1/2 MS containing 4 µM FM4-64 and 25 µM BFA in the dark for 10 minutes before imaging or for 10 minutes in 1/2 MS with 4 µM FM4-64 and 25 µM BFA in the dark before washing and incubating in 1/2 MS with 25 µM BFA for 50 minutes before imaging. Images were single slices, taken of epidermal cells in the root elongation zone. A ratio of internal/PM signal was measured in imageJ by using the polygon selection tool to measure the mean grey value of the entire

interior of the cell and divide this by the PM mean grey value, acquired using the segmented line tool (width 1).

Trafficking of FM4-64 to the tonoplast was measured by incubating plants in 1/2 MS containing 4 µM FM4-64 for 10 minutes before washing and incubating in 1/2 MS for 3 hours. Images were single slices taken of epidermal cells in the root elongation zone. A ratio of tonoplast/PM signal was acquired using the segmented line tool for both PM and tonoplast measurement.

Exocytosis was assayed in the root tips of 6 day old plants using PIN2-GFP or LTI6b-GFP in the epidermis. For the "T0" image point, plants were taken directly off growth media and immediately imaged. Otherwise, plants were treated with 25 µM BFA for 60 minutes, at which point some plants were imaged to obtain the "60' BFA" images. The rest were washed in liquid 1/2 MS and left to recover for 60 minutes in liquid 1/2 MS media before imaging for the "60' washout" images. Signal internalisation was measured as described for endocytosis. Imaging was done with the 60x objective and Nikon A1R Confocal Laser-Scanning microscope described above.

Acknowledgments

We thank Melanie Krebs for providing seeds expressing the TGN/EE pH sensor. Matthew Tucker for the 3xVenusNLS plasmid, Steve Tyerman for helpful discussions, Philip Brewer for PIN2::PIN2-GFP seeds and Christian Luschnig for advice on genotyping. We thank Renée Philips and Marie Beillevert for assistance with lab and plant work. We thank Adelaide Microscopy, especially Gwen Mayo and Jane Sibbons, for support with microscopy; and we thank the University of Melbourne Advanced Microscopy Facility where Electron microscopy was conducted. We thank the Australian Research Council for funding this work through DE170100054 to HEM, FT130100709 and CE140100008 to M.G., and DE160100804 to S.W.; HEM is also supported in part by funding from the CRC program as the Canada Research Chair in Plant Cell Biology.

Author contributions

SW led the project; DWM, MG and SW designed experiments; DWM conducted most experiments with contributions from SW, HEM, YQ and AS; DWM, MG and SW wrote the paper, HEM, AS and YQ commented on the paper.

References

Adamowski M, Friml J (2015) PIN-Dependent Auxin Transport: Action, Regulation, and Evolution. Plant Cell **27:** 20-32

Barberon M, Zelazny E, Robert S, Conejero G, Curie C, Friml J, Vert G (2011) Monoubiquitin-dependent endocytosis of the IRON-REGULATED TRANSPORTER 1 (IRT1) transporter controls iron uptake in plants. Proceedings of the National Academy of Sciences of the United States of America **108:** E450-E458

Bassil E, Ohto M-a, Esumi T, Tajima H, Zhu Z, Cagnac O, Belmonte M, Peleg Z, Yamaguchi T, Blumwald E (2011) The Arabidopsis intracellular Na^+/H^+ antiporters NHX5 and NHX6 are endosome associated and necessary for plant growth and development. Plant Cell **23:** 224-239

Bolte S, Cordelieres FP (2006) A guided tour into subcellular colocalization analysis in light microscopy. Journal of Microscopy **224:** 213-232

Brux A, Liu TY, Krebs M, Stierhof YD, Lohmann JU, Miersch O, Wastermack C, Schumacher K (2008) Reduced V-ATPase activity in the trans-Golgi network causes oxylipin-dependent hypocotyl growth inhibition in Arabidopsis. Plant Cell **20:** 1088-1100

Chen ZC, Yamaji N, Fujii-Kashino M, Ma JF (2016) A cation-chloride cotransporter gene Is required for cell elongation and osmoregulation in rice. Plant Physiology **171:** 494-507

Colmenero-Flores JM, Martínez G, Gamba G, Vázquez N, Iglesias DJ, Brumós J, Talón M (2007) Identification and functional characterization of cation–chloride cotransporters in plants. Plant Journal **50:** 278-292

Cutler S, R. , Ehrhardt D, W., Griffitts J, S., Somerville C, R. (2000) Random GFP::cDNA fusions enable visualization of subcellular structures in cells of *Arabidopsis* at a high frequency. Proceedings of the National Academy of Sciences **97:** 3718-3723

Dettmer J, Hong-Hermesdorf A, Stierhof Y-D, Schumacher K (2006) Vacuolar H^+-ATPase activity is required for endocytic and secretory trafficking in *Arabidopsis*. Plant Cell **18:** 715-730

Domingos P, Dias PN, Tavares B, Portes MT, Wudick MM, Konrad KR, Gilliham M, Bicho A, Feijó JA (2019) Molecular and electrophysiological characterization of anion transport in *Arabidopsis thaliana* pollen reveals regulatory roles for pH, $Ca2^+$ and GABA. New Phytologist **223:** 1353-1371

Dragwidge JM, Ford BA, Ashnest JR, Das P, Gendall AR (2018) Two endosomal NHX-Type Na^+/H^+ antiporters are involved in auxin-mediated development in *Arabidopsis thaliana*. Plant and Cell Physiology **59:** 1660-1669

Dragwidge JM, Scholl S, Schumacher K, Gendall AR (2019) NHX-type $Na^+(K^+)/H^+$ antiporters are required for TGN/EE trafficking and endosomal ion homeostasis in Arabidopsis thaliana. Journal of Cell Science **132**

Geldner N, Friml J, Stierhof YD, Jurgens G, Palme K (2001) Auxin transport inhibitors block PIN1 cycling and vesicle traficking. Nature **413:** 425-428

Gilles JF, Dos Santos M, Boudier T, Bolte S, Heck N (2017) DiAna, an ImageJ tool for object-based 3D co-localization and distance analysis. Methods **115:** 55-64

Guan R, Qu Y, Guo Y, Yu L, Liu Y, Jiang J, Chen J, Ren Y, Liu G, Tian L, Jin L, Liu Z, Hong H, Chang R, Gilliham M, Qiu L (2014) Salinity tolerance in soybean is modulated by natural variation in *GmSALT3*. Plant Journal **80:** 937-950

543 **Guo W, Zuo Z, Cheng X, Sun J, Li H, Li L, Qiu J-L** (2014) The chloride channel family gene *CLCd*
544 negatively regulates pathogen-associated molecular pattern (PAMP)-triggered immunity in
545 *Arabidopsis*. Journal Of Experimental Botany **65:** 1205-1215
546 **Han BD, Jiang YH, Cui GX, Mi JN, Roelfsema MRG, Mouille G, Sechet J, Al-Babili S, Aranda M, Hirt H**
547 (2020) CATION-CHLORIDE CO-TRANSPORTER 1 (CCC1) Mediates Plant Resistance against
548 *Pseudomonas syringae*. Plant Physiology **182:** 1052-1065
549 **Henderson S, Wege S, Gilliham M** (2018) Plant cation-chloride cotransporters (CCC): evolutionary
550 origins and functional insights. International Journal of Molecular Sciences **19:** 492
551 **Henderson SW, Wege S, Qiu J, Blackmore DH, Walker AR, Tyerman SD, Walker RR, Gilliham M**
552 (2015) Grapevine and Arabidopsis cation-chloride cotransporters localize to the Golgi and
553 trans-Golgi network and indirectly influence long-distance ion transport and plant salt
554 tolerance. Plant Physiology **169:** 2215-2229
555 **Jefferson RA, Kavanagh TA, Bevan MW** (1987) GUS fusions: beta-glucuronidase as a sensitive and
556 versatile gene fusion marker in higher plants. EMBO journal **6:** 3901-3907
557 **Johnson M, Zhou Q, Smith E** (2004) Arabidopsis *hapless* mutations define essential gametophytic
558 functions. Genetics **168:** 971-982
559 **Luo Y, Scholl S, Doering A, Zhang Y, Irani NG, Rubbo SD, Neumetzler L, Krishnamoorthy P, Van**
560 **Houtte I, Mylle E, Bischoff V, Vernhettes S, Winne J, Friml J, Stierhof Y-D, Schumacher K,**
561 **Persson S, Russinova E** (2015) V-ATPase-activity in the TGN/EE is required for exocytosis and
562 recycling in *Arabidopsis*. Nature Plants **1:** 15094
563 **Marmagne A, Vinauger-Douard M, Monachello D, de Longevialle AF, Charon C, Allot M, Rappaport**
564 **F, Wollman FA, Barbier-Brygoo H, Ephritikhine G** (2007) Two members of the Arabidopsis
565 CLC (chloride channel) family, AtCLCe and AtCLCf, are associated with thylakoid and Golgi
566 membranes, respectively. Journal of Experimental Botany **58:** 3385-3393
567 **Marques-Bueno MM, Morao AK, Cayrel A, Platre MP, Barberon M, Caillieux E, Colot V, Jaillais Y,**
568 **Roudier F, Vert G** (2016) A versatile Multisite Gateway-compatible promoter and transgenic
569 line collection for cell type-specific functional genomics in Arabidopsis. Plant Journal **85:** 320-
570 333
571 **Martinière A, Bassil E, Jublanc E, Alcon C, Reguera M, Sentenac H, Blumwald E, Paris N** (2013) In
572 vivo intracellular pH measurements in tobacco and *Arabidopsis* reveal an unexpected pH
573 gradient in the endomembrane system. Plant Cell **25:** 4028-4043
574 **McDowell SC, Akmakjian G, Sladek C, Mendoza-Cozatl D, Morrissey JB, Saini N, Mittler R, Baxter I,**
575 **Salt DE, Ward JM, Schroeder JI, Guerinot ML, Harper JF** (2013) Elemental Concentrations in
576 the Seed of Mutants and Natural Variants of *Arabidopsis thaliana* Grown under Varying Soil
577 Conditions. Plos One **8**
578 **Nikolovski N, Rubtsov D, Segura MP, Miles GP, Stevens TJ, Dunkley TPJ, Munro S, Lilley KS, Dupree**
579 **P** (2012) Putative Glycosyltransferases and Other Plant Golgi Apparatus Proteins Are
580 Revealed by LOPIT Proteomics. Plant Physiology **160:** 1037-1051
581 **Novarino G, Weinert S, Rickheit G, Jentsch TJ** (2010) Endosomal Chloride-Proton Exchange Rather
582 Than Chloride Conductance Is Crucial for Renal Endocytosis. Science **328:** 1398-1401
583 **Reguera M, Bassil E, Tajima H, Wimmer M, Chanoca A, Otegui MS, Paris N, Blumwald E** (2015) pH
584 Regulation by NHX-Type Antiporters Is Required for Receptor-Mediated Protein Trafficking
585 to the Vacuole in Arabidopsis. Plant Cell **27:** 1200-1217
586 **Schindelin J, Arganda-Carreras I, Frise E, Kaynig V, Longair M, Pietzsch T, Preibisch S, Rueden C,**
587 **Saalfeld S, Schmid B, JTinevez e-Y, White DJ, Hartenstein V, Eliceiri K, Tomancak P, Cardona**
588 **A** (2012) Fiji: an open-source platform for biological-image analysis. Nature Methods **9:** 676-
589 682
590 **Schoenaers S, Balcerowicz D, Breen G, Hill K, Zdanio M, Mouille G, Holman TJ, Oh J, Wilson MH,**
591 **Nikonorova N, Vu LD, De Smet I, Swarup R, De Vos WH, Pintelon I, Adriaensen D, Grierson**
592 **C, Bennett MJ, Vissenberg K** (2018) The auxin-regulated CrRLK1L kinase *ERULUS* controls cell
593 wall composition during root hair tip growth. Current Biology **28:** 722-732

Schumacher K, Vafeados D, McCarthy M, Sze H, Wilkins T, Chory J (1999) The Arabidopsis *det3* mutant reveals a central role for the vacuolar H^+-ATPase in plant growth and development. Genes & Development **13:** 3259-3270

Sinclair R, Rosquete MR, Drakakaki G (2018) Post-Golgi Trafficking and Transport of Cell Wall Components. Frontiers in Plant Science **9**

Sliwinska E, Mathur J, Bewley JD (2015) On the relationship between endoreduplication and collet hair initiation and tip growth, as determined using six *Arabidopsis thaliana* root-hair mutants Journal Of Experimental Botany **66:** 3285-3295

Sze H, Chanroj S (2018) Plant endomembrane dynamics: studies of K^+/H^+ antiporters provide insights on the effects of pH and ion homeostasis. Plant Physiology **177:** 875-895

Viotti C, Bubeck J, Stierhof YD, Krebs M, Langhans M, van den Berg W, van Dongen W, Richter S, Geldner N, Takano J, Jurgens G, de Vries SC, Robinson DG, Schumacher K (2010) Endocytic and Secretory Traffic in Arabidopsis Merge in the Trans-Golgi Network/Early Endosome, an Independent and Highly Dynamic Organelle. Plant Cell **22:** 1344-1357

von der Fecht-Bartenbach J, Bogner M, Krebs M, Stierhof Y-D, Schumacher K, Ludewig U (2007) Function of the anion transporter AtCLC-d in the *trans*-Golgi network. Plant Journal **50:** 466-474

Wang Y, Tang R-J, Yang X, Zheng X, Shao Q, Tang Q-L, Fu A, Luan S (2019) Golgi-localized cation/proton exchangers regulate ionic homeostasis and skotomorphogenesis in *Arabidopsis*. Plant, Cell & Enviroment **42:** 673-687

Wegner LH (2017) Cotransport of water and solutes in plant membranes: The molecular basis, and physiological functions. Aims Biophysics **4:** 192-209

Wendrich JR, Yang B, Vandamme N, Verstaen K, Smet W, Van de Velde C, Minne M, Wybouw B, Mor E, Arents HE, Nolf J, Van Duyse J, Van Isterdael G, Maere S, Saeys Y, De Rybel B (2020) Vascular transcription factors guide plant epidermal responses to limiting phosphate conditions. Science **370:** eaay4970

Xu J, Scheres B (2005) Dissection of Arabidopsis ADP-RIBOSYLATION FACTOR 1 function in epidermal cell polarity. Plant Cell **17:** 525-536

Zhang GF, Driouich A, Staehelin LA (1993) Effects of monensin on plant Golgi: re-examination of monensin-induced changes in cisternal architecture and functional activities of the Golgi apparatus of sycamore suspension-cultured cells. Journal of Cell Science **104:** 819-831

Figure legends

Figure 1. *AtCCC1* is expressed in the majority of cell types. Expression of either 3xVenusNLS (bright YFP variant with a nuclear localisation signal) or β-glucuronidase (blue GUS staining). A-H) 3xVenusNLS expression indicating promoter activity in all root cells, including the root tip and root hairs, and hypocotyl, leaf cells including trichomes and guard cells, as well as stigma and stamen tissue. I-M) GUS staining indicating promoter activity predominantly in younger leaves, floral stem, stamen stigma and root stele. Scale bars are 50 µm (images A-B, G), 100 µm (images C-D, H, J), 5 µm (image E), 20 µm (image F), 5 mm (image I), 200 µm (images K, M) and 1000 µm (image L).

Figure 2. AtCCC1 is important for cell elongation. A-B) Root epidermal cells are shorter in *Atccc1*. n > 13 cells. Images are maximum intensity projections of cell wall autofluorescence. Scale bars are 50 µm. C-D) *Atccc1* has shorter root hairs. n > 900 root hairs of > 30 plants. Scale bars are 100 µm. E) *Atccc1* plant do not develop collet hairs. Scale bars are 500 µm F) *Atccc1* root hairs elongate more slowly (See supplementary videos 1 and 2). Boxplots show range excluding outliers; median and 1st and 3rd quartile are indicated. Points represent individual measurements. Students t-tests comparing *Atccc1* to wildtype. ** indicates $P<0.01$, **** indicates $P<0.0001$

Figure 3. Functional GFP-AtCCC1 is localised in the TGN/EE. A-B) Expression of *GFP-AtCCC1* in trichoblasts rescues *Atccc1* root hair length defects. n > 1300 root hairs. Scale bars are 100 µm C) GFP-AtCCC1 (green) and VHAa1-RFP (magenta) colocalise in trichoblast cells. Colocalisation was calculated using DiAna object based colocalisation plugin in ImageJ. Error is standard deviation. n = 15 cells of 5 plants. Scale bars are 10 µm. Images are a single optical section from a stack. Boxplot shows range excluding outliers; median and 1st and 3rd quartile are indicated. Students t-tests comparing genotypes to wildtype. **** indicates $P<0.0001$

Figure 4. AtCCC1 is required for regulation of TGN/EE luminal conditions. A-B) TGN/EE swelling is more severe in *Atccc1* epidermal root cell in response to 15 minutes treatment with 2.5 µM monensin. TGN/EE are visualised by VHAa1-RFP (white). n > 28

plants. Scale bars are 10 µm. Images are a single optical section. C-D) The pH of *Atccc1* TGN/EE is 0.3 units higher compared to wildtype. Images show the ratio of GFP/RFP of the pH-sensor SYP61-pHusion in the TGN/EE lumen. n > 26 plants. Scale bars are 10 µm. Boxplots show range excluding outliers; median and 1st and 3rd quartile are indicated. Points represent individual measurements. Students t-tests comparing *Atccc1* to wildtype. * indicates $P < 0.05$, **** indicates $P < 0.0001$

Figure 5. AtCCC1 is important for endomembrane trafficking. A-B) *Atccc1* root epidermal cells show a reduced recovery of PIN2-GFP (green) cytoplasmic/PM signal ratio after a 60 minute treatment with 25 µM BFA. n > 24 cells, 3 cells measured per plant. C-D) Endocytosis of the membrane dye FM4-64 (red) is reduced in *Atccc1*. Endocytosis of FM4-64 is measured as an increase in the cytoplasm/PM ratio. Plants were kept in 25 µM BFA for the duration of the experiment. n > 56 cells of > 9 plants. E-F) Endocytosis and trafficking of FM4-64 (red) to the vacuole in the absence of BFA is reduced in *Atccc1*. Accumulation of FM4-64 at the tonoplast is measured as an increase of the tonoplast/PM ratio. n > 51 cells of > 18 plants. Boxplots show range excluding outliers; median and 1st and 3rd quartile are indicated. Points represent individual measurements. All images are a single optical section. Students t-tests comparing *Atccc1* to wildtype. ** indicates $P < 0.01$, **** indicates $P < 0.0001$ All scale bars are 10 µm.

Figure 6: Proposed model of ion and pH regulation in the TGN/EE. The H^+-V-ATPase proton pump, the cation-proton exchangers NHX5 and NHX6 and the anion-proton exchanger CLCd have been previously shown or proposed to be important for pH regulation in the TGN/EE lumen. CCC1s are candidates for providing an electroneutral cation and anion efflux mechanism, completing the regulatory transport circuit.

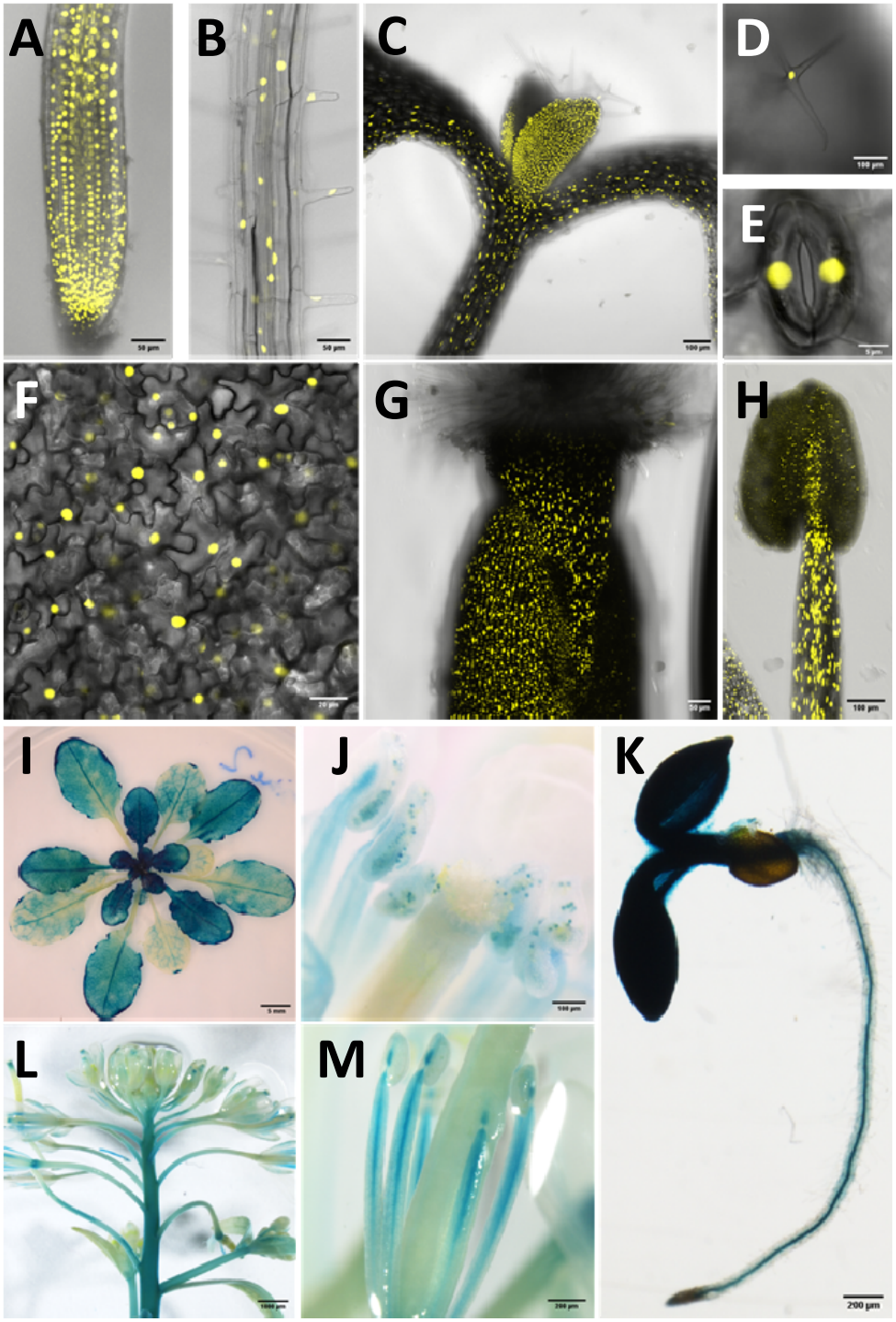

Figure 1. *AtCCC1* is expressed in the majority of cell types. Expression of either 3xVenusNLS (bright YFP variant with a nuclear localisation signal) or β-glucuronidase (blue GUS staining). A-H) 3xVenusNLS expression indicating promoter activity in all root cells, including the root tip and root hairs, and hypocotyl, leaf cells including trichomes and guard cells, as well as stigma and stamen tissue. I-M) GUS staining indicating promoter activity predominantly in younger leaves, floral stem, stamen stigma and root stele. Scale bars are 50 µm (images A-B, G), 100 µm (images C-D, H, J), 5 µm (image E), 20 µm (image F), 5 mm (image I), 200 µm (images K, M) and 1000 µm (image L).

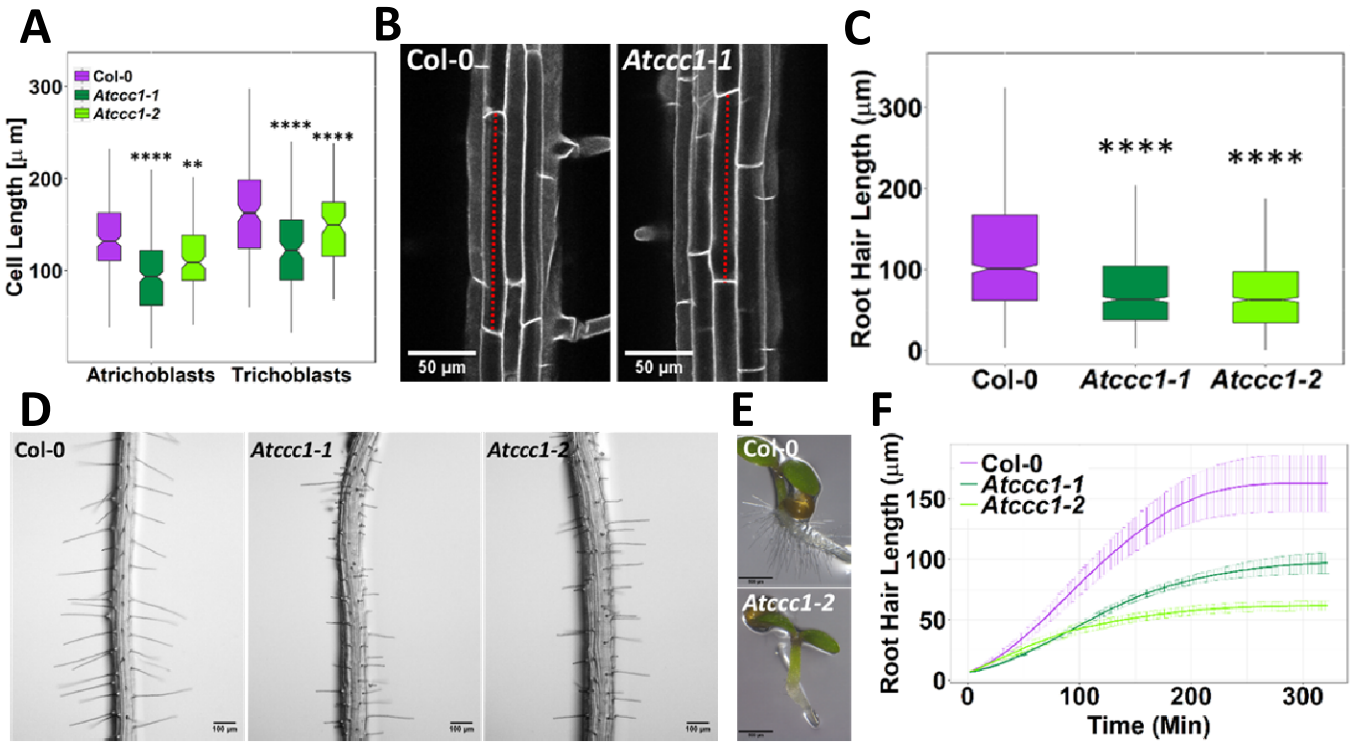

Figure 2. AtCCC1 is important for cell elongation. A-B) Root epidermal cells are shorter in *Atccc1*. n > 13 cells. Images are maximum intensity projections of cell wall autofluorescence. Scale bars are 50 µm. C-D) *Atccc1* has shorter root hairs. n > 900 root hairs of > 30 plants. Scale bars are 100 µm. E) *Atccc1* plant do not develop collet hairs. Scale bars are 500 µm F) *Atccc1* root hairs elongate more slowly (See supplementary videos 1 and 2). Boxplots show range excluding outliers; median and 1st and 3rd quartile are indicated. Points represent individual measurements. Students t-tests comparing *Atccc1* to wildtype. ** indicates $P<0.01$, **** indicates $P<0.0001$

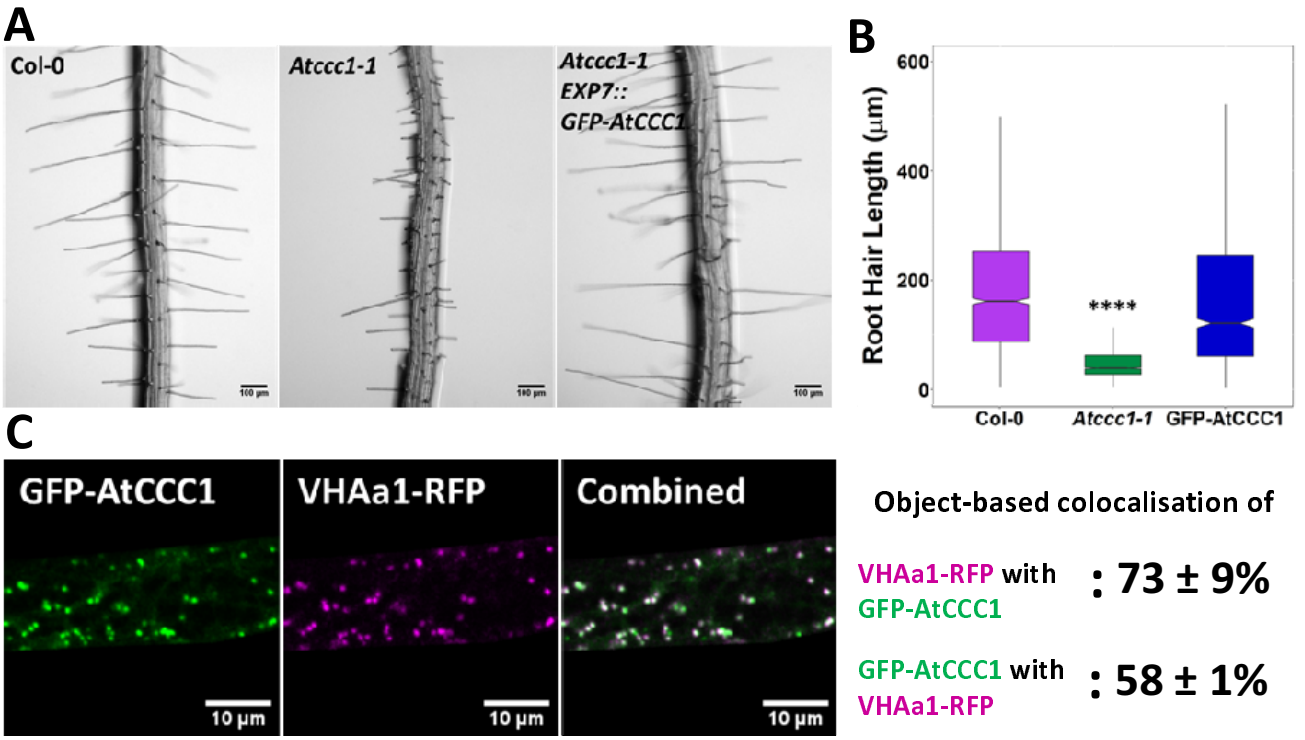

Figure 3. Functional GFP-AtCCC1 is localised in the TGN/EE. A-B) Expression of *GFP-AtCCC1* in trichoblasts rescues *Atccc1* root hair length defects. n > 1300 root hairs. Scale bars are 100 µm C) GFP-AtCCC1 (green) and VHAa1-RFP (magenta) colocalise in trichoblast cells. Colocalisation was calculated using DiAna object based colocalisation plugin in ImageJ. Error is standard deviation. n = 15 cells of 5 plants. Scale bars are 10 µm. Images are a single optical section from a stack. Boxplot shows range excluding outliers; median and 1st and 3rd quartile are indicated. Students t-tests comparing genotypes to wildtype. **** indicates $P<0.0001$

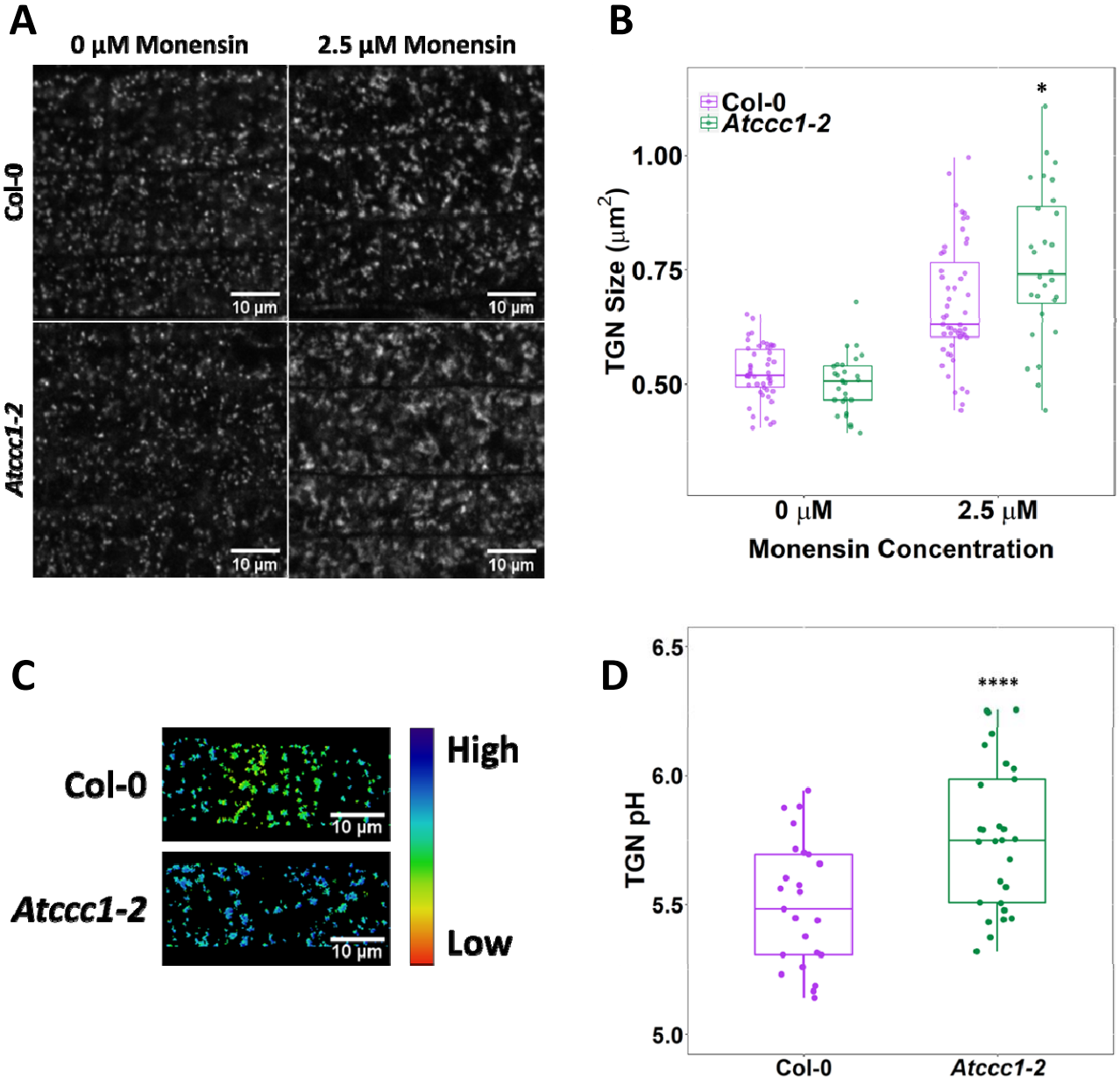

Figure 4. AtCCC1 is required for regulation of TGN/EE luminal conditions. A-B) TGN/EE swelling is more severe in *Atccc1* epidermal root cell in response to 15 minutes treatment with 2.5 µM monensin. TGN/EE are visualised by VHAa1-RFP (white). n > 28 plants. Scale bars are 10 µm. Images are a single optical section. C-D) The pH of *Atccc1* TGN/EE is 0.3 units higher compared to wildtype. Images show the ratio of GFP/RFP of the pH-sensor SYP61-pHusion in the TGN/EE lumen. n > 26 plants. Scale bars are 10 µm. Boxplots show range excluding outliers; median and 1st and 3rd quartile are indicated. Points represent individual measurements. Students t-tests comparing *Atccc1* to wildtype. * indicates $P < 0.05$, **** indicates $P < 0.0001$

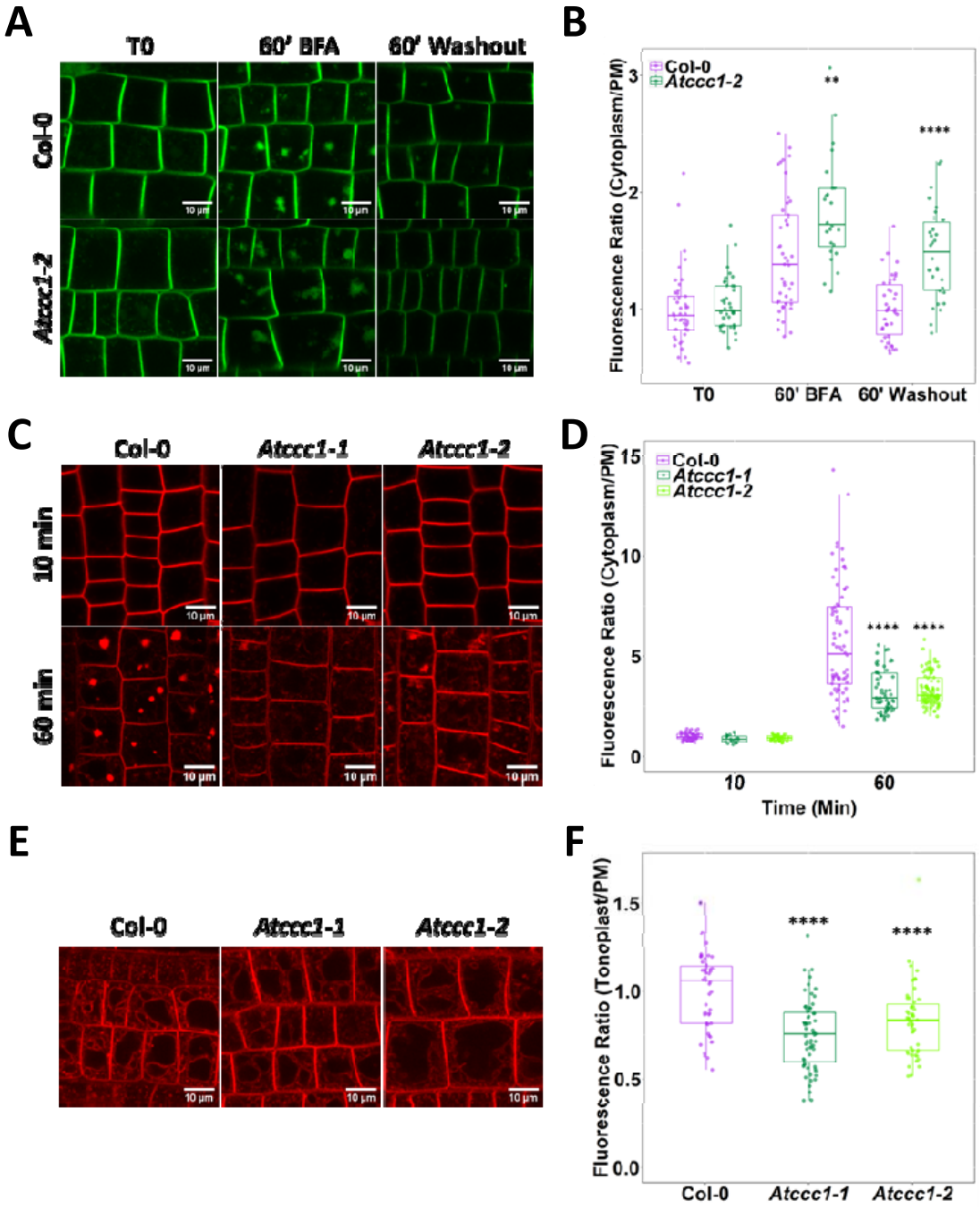

Figure 5. AtCCC1 is important for endomembrane trafficking. A-B) *Atccc1* root epidermal cells show a reduced recovery of PIN2-GFP (green) cytoplasmic/PM signal ratio after a 60 minute treatment with 25 µM BFA. n > 24 cells, 3 cells measured per plant. C-D) Endocytosis of the membrane dye FM4-64 (red) is reduced in *Atccc1*. Endocytosis of FM4-64 is measured as an increase in the cytoplasm/PM ratio. Plants were kept in 25 µM BFA for the duration of the experiment. n > 56 cells of > 9 plants. E-F) Endocytosis and trafficking of FM4-64 (red) to the vacuole in the absence of BFA is reduced in *Atccc1*. Accumulation of FM4-64 at the tonoplast is measured as an increase of the tonoplast/PM ratio. n > 51 cells of > 18 plants. Boxplots show range excluding outliers; median and 1st and 3rd quartile are indicated. Points represent individual measurements. All images are a single optical section. Students t-tests comparing *Atccc1* to wildtype. ** indicates $P < 0.01$, **** indicates $P < 0.0001$ All scale bars are 10 µm.

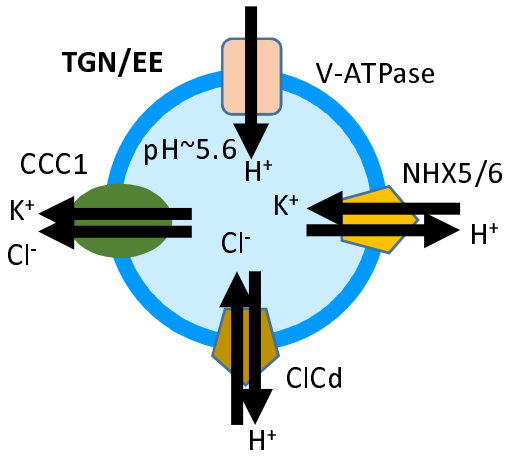

Figure 6: Proposed model of ion and pH regulation in the TGN/EE. The H^+-V-ATPase proton pump, the cation-proton exchangers NHX5 and NHX6 and the anion-proton exchanger CLCd have been previously shown or proposed to be important for pH regulation in the TGN/EE lumen. CCC1s are candidates for providing an electroneutral cation and anion efflux mechanism, completing the regulatory transport circuit.